The ontogeny of masticatory muscle architecture in Microcebus murinus

Kaitlyn Leonard, Marissa Boettcher, Edwin Dickinson, Neha Malhotra, Fabienne Aujard, Anthony Herrel, Adam Hartstone-rose

Leonard Kaitlyn (Orcid ID: 0000-0002-5380-6740)
Hartstone-Rose Adam (Orcid ID: 0000-0001-5307-5573)

The ontogeny of masticatory muscle architecture in *Microcebus murinus*

Kaitlyn C. Leonard[1], Marissa L. Boettcher[1], Edwin Dickinson[1], Neha Malhotra[2], Fabienne Aujard[3], Anthony Herrel[3], Adam Hartstone-Rose[1]

Institutional Affiliation: [1]Department of Biological Sciences, North Carolina State University, [2]University of South Carolina School of Medicine, [3]UMR7179 CNRS/MNHN, 55 rue Buffon, 75005 Paris, France.

Corresponding Author: Kaitlyn Leonard, North Carolina State University. Telephone: (919) 515-1761; Fax: 919-515-3355; Email: kcleona2@ncsu.edu

Running Title: Masticatory ontogeny of *Microcebus murinus*

Grant Information: Grant sponsor: National Science Foundation; Grant numbers: IOS-15-57125 and BCS-14-40599.

ABSTRACT

The masticatory apparatus has been the focus of many studies in comparative anatomy – especially analyses of skulls and teeth, but also of the mandibular adductor muscles which are responsible for the production of bite force and the movements of the mandible during food processing and transport. The fiber architecture of these muscles has been correlated to specific diets (e.g., prey size in felids) and modes of foraging (e.g., tree gouging in marmosets). Despite the well-elucidated functional implications of this architecture, little is known about its ontogeny. To characterize age-related myological changes, we studied the masticatory muscles in a large (n=33) intraspecific sample of a small, Malagasy primate, *Microcebus murinus* including neonatal through geriatric individuals. We removed each of the mandibular adductors and recorded its mass as well as other linear measurements. We then chemically dissected each muscle to study its architecture – fascicle length and physiological cross-sectional area (PCSA) which relate to stretch (gape) and force capabilities respectively. We observed PCSA and muscle mass to increase rapidly and plateau in adulthood through senescence. Fascicle lengths remained relatively constant once maximal length was reached, which occurred early in life, suggesting that subsequent changes in PCSA are driven by changes in muscle mass. Quadratic curvilinear models of each of the architectural variables of all adductors combined as well as individual muscles regressed against age were all significant.

KEYWORDS: mastication, development, senescence, growth, muscle atrophy

INTRODUCTION

The arrangement of muscle fascicles within the masticatory apparatus has been shown to correlate with dietary adaptations in both primates (Perry and Wall, 2008; Eng et al., 2009; Taylor and Vinyard, 2009; Perry and Hartstone-Rose, 2010; Perry et al., 2011; Perry et al., 2014; Hartstone-Rose et al., 2018) and other mammals(Taylor et al., 2006; Herrel et al., 2008; Hartstone-Rose et al., 2012; Santana and Cheung, 2016; Fabre et al., 2017; Curtis and Santana, 2018; Santana, 2018). Despite our understanding of the relationship between fascicular architecture and masticatory function, however, few studies have considered how this architecture changes throughout the lifetime of an animal (Huhov et al., 1988; Langenbach and Weijs, 1990; Pfaller et al., 2009; Pfaller et al., 2011), especially within the primate order (though see Dickinson et al., 2018). Importantly, characterizing the architectural properties of muscles at various stages of life could provide valuable insights into dynamic functional demands throughout ontogeny and its impact upon the masticatory apparatus.

The functionality of a particular muscle is directly related to its architectural properties. A muscle of a given volume can be highly pennate and therefore optimized for maximal force production. Alternatively, muscles may have no pennation and long fibers and therefore, are optimized for maximal stretch and speed (Gans and Bock, 1965; Gans, 1982; Otten, 1988; Gans and Gaunt, 1991; Anapol and Barry, 1996; Lieber and Friden, 2000). Muscles may also fall somewhere along this continuum between highly pennate and not pennate at all (i.e.,

intermediary amounts of pennation; Anapol and Barry, 1996; Lieber and Friden, 2000). This architecture is studied by analyzing the configuration of the muscle fascicles (e.g., Gans and Bock, 1965), which are bundles of individual muscle fibers. For a given muscle fiber type, total force producing capacity is directly correlated with a muscle's cross-sectional area (i.e., thicker muscles comprised of more fiber bundles in parallel are stronger). Muscle fibers themselves are comprised of serially arranged sarcomeres, which shorten during contraction. As longer muscle fibers are comprised of more sarcomeres, they are capable of both greater contractile velocity and greater total excursion. These same principals are generalizable to the bundles of fibers—fascicles.

The reason that muscles of a given volume can be optimized for either maximal force production or maximal stretch and speed relates to the distribution of fascicles therein: to maximize fascicle length, muscle fibers should be arranged in parallel, spanning the entire length of the muscle along the muscle's line of action from origin to insertion such that each muscle fascicle is roughly equivalent to the length of the whole muscle (Gans and Bock, 1965). By arranging fascicles in a pennate configuration, by contrast, more fascicles can be accommodated within a muscle's volume; however, packing more fibers into the same volume means that each is relatively shorter, typically spanning from the muscle's medial or lateral border to a central tendon (Gans, 1982; Anapol and Barry, 1996).

Previously, it has been determined that cross-sectional area is directly proportional to maximal force production capabilities (Knuttgen, 1976; Maughan et al., 1983). However, this is

not the case in instances of pennate muscles—muscles with fascicles with an angular arrangement (Leischner et al., 2018). To accurately account for fascicular orientation, a cross-sectional area is taken that is perpendicular to all muscle fascicles—a variable known as physiological cross-sectional area (PCSA). Physiological cross-sectional area is a function of mass, fascicle length and the specific density of muscle (Schumacher, 1961). Often PCSA is "reduced" (RPCSA) to include only the force of pull along the muscle's line of action (i.e., the perpendicular vector of these angular pennate fibers is removed) – especially for limb muscles that are long, straight and move along one clear line of action (Anapol and Barry, 1996). However, the masticatory muscles are rotational (i.e., they move the mandible along an arc, not in a straight line) and each individually have angularity in multiple planes in ever changing axes (Hartstone-Rose et al., 2018).

Muscles of mastication and their fascicular architecture have been well studied and while the abducting digastric muscles and the anterior translator, the lateral pterygoid are important for chewing, it is the mandibular adductors that have been the central focus (though see Curtis and Santana, 2018). The mandibular adductors include the masseter, temporalis, and medial pterygoid and have been of particular interest within anatomical research because their architecture correlates with bite force and diet (Taylor et al., 2006; Anapol et al., 2008; Perry and Wall, 2008; Perry et al., 2011; Hartstone-Rose et al., 2012; Perry et al., 2014; Fabre et al., 2017; Hartstone-Rose et al., 2018; Santana, 2018).

For instance, Hartstone-Rose and colleagues (2012) observed that muscle fascicle lengths in felids are correlated with relative prey size. That is, cats that exploit relatively large prey (e.g., herbivores that are larger than the predators themselves) have relatively longer masticatory muscle fascicles whereas cat species that specialize in relatively small prey (e.g., small rodents) have relatively short muscle fascicles. Other similar findings have related the architectural properties of the masticatory muscles to carnivory in bats (Santana and Cheung, 2016), food size and diet in bats (Dumont et al., 2009; Curtis and Santana, 2018; Santana, 2018), dietary consistency in rabbits (Taylor et al., 2006) and carnivory in water-rats (Fabre et al., 2017).

The muscle architecture of the masticatory apparatus has also been the focus of considerable research within the primate order (Antón, 1999; Antón, 2000; Anapol et al., 2008; Perry and Wall, 2008; Eng et al., 2009; Taylor and Vinyard, 2009; Perry and Hartstone-Rose, 2010; Perry et al., 2011; Perry et al., 2014; Hartstone-Rose et al., 2018). From these inquiries we have a better understanding of 1) the uniformity within different portions of the masticatory muscles (Antón, 1999), 2) the way that masticatory muscles are adapted to overcome mechanically disadvantaged leverages (e.g., prognathic faces; Antón, 1999; Antón, 2000), 3) the allometric scaling of the architectural properties of masticatory muscles (Anapol et al., 2008; Perry and Wall, 2008; Perry et al., 2011; Hartstone-Rose et al., 2018), and 4) the correlations between masticatory muscle architecture and dietary processing and acquisition (Eng et al., 2009; Taylor and Vinyard, 2009; Perry et al., 2014; Hartstone-Rose et al., 2018). However, only a few studies of primates have sought to clarify how these architectural properties might develop

and change throughout the life of the animal (Carlson, 1983; Cachel, 1984; Dickinson et al., 2018; Prufrock and Perry, 2018).

Through the use of radiopaque markers embedded into portions of the developing masseter within female immature rhesus macaques (*Macaca mulatta*), it was observed that the masseter underwent elongation throughout ontogeny (Carlson, 1983). This phenomenon was attributed to the addition of sarcomeres during development (Carlson, 1983). A more comprehensive interspecific study conducted by Cachel (1984) investigated growth and allometry in primate masticatory muscles on the basis of dry muscle weights, determining that the mass of the masticatory muscles scaled isometrically with body mass during development. However, architectural properties of these muscles were not considered. More recently Dickinson and colleagues (2018) investigated ontogenetic changes in muscle architecture across the adductor musculature of the crab-eating macaque (*M. fascicularis*). They observed that muscle mass, PCSA and fascicle lengths scaled with positive allometry relative to both jaw length and condyle-molar length across the life span of their focal species (Dickinson et al., 2018).

Ontogeny within Microcebus murinus

The grey mouse lemur, *Microcebus murinus*, is a small nocturnal primate native to Western Madagascar (Mittermeier et al., 2010). Due to its small size and manageability –

especially for a primate – it exists as a model organism in numerous colonies across Europe and the United States (Martin, 1971; Rassoul et al., 2010; Ezran et al., 2017) in larger numbers than most other primate species. The life span for these animals in the field has been reported to be between three and four years (Bons et al., 2006); however, in captive environments they tend to live to be around five years of age with a maximal lifespan of up to eleven years. (Perret, 1997; Castanet et al., 2004). They are weaned around two months of age, reach their adult mass by six months (Castanet et al., 2004) and are sexually mature by around nine months (Lutermann et al., 2006). Individuals older than five years of age are considered to be senescent within this species (Bons et al., 2006).

In addition to their manageability and relatively short lifespans, another characteristic of *M. Murinus* making them an ideal model system is their rather generalized diet. Mouse lemurs in the consume a wide array of foods consisting of fruit, insects, gum, and some small vertebrates (Dammhahn and Kappeler, 2008). A recent study into the ontogeny of bite force in this species identified a strong positive correlation between *in vivo* bite force and age within *M. murinus* (Chazeau et al., 2012). The authors report that older individuals were capable of generating greater bite forces than their younger counterparts. However, their oldest age group (5.5 years), demonstrated a decline in force production relative to prime-age adults (Chazeau et al., 2012), suggesting that bite force may decline in senescent individuals.

Aims and predictions

Following previous studies conducted on the ontogeny of primate mastication, this study aims to quantify ontogenetic changes to the size and architecture of the jaw-adductor musculature in *M. murinus* using the largest intraspecific study in primates to date. While an *in vivo* study pertaining to the ontogeny of bite force in *M. murinus* has been previously conducted by Chazeau and colleagues (2012), this study specifically focuses on the age-associated anatomical changes of the mandibular adductors and includes individuals more advanced in age, which may further elucidate the functional changes they observed. On the basis of this previous work, in addition to recent studies into the life history and bite force potential of this species, we hypothesize the following:

H1: PCSA increases throughout ontogeny, driven by an increase in muscle mass, as the functional demands on the masticatory musculature change from suckling to chewing.

As an organism makes the transition from suckling to chewing solid foods, additional adductive force is needed. This requires greater PCSA or potentially more orthognathic faces (i.e., greater mechanical advantage). Increasing PCSA requires either an increase in muscle mass or a reduction in fascicle length (because, for the same volume, a muscle with shorter fascicles has *more* fascicles and therefore a greater PCSA). As a reduction in fascicle length would reduce the maximal possible gape distance (unlikely, given that masticating animals would be required

to attain larger gapes than suckling infants), this increase in force capacity is likely to be driven by an increase in overall muscle mass and volume.

H2: Muscle mass and PCSA decline at onset of senescence at 5.5 years of age.

A recent study conducted by Chazeau and colleagues (2012) reports that whereas bite force is strongly correlated with age with in *M. murinus*, the oldest age group within their study, which was 5.5 years of age, experienced a decline in force production relative to younger adults (Chazeau et al., 2012). They suggested that the decline observed may be due to age-associated muscle atrophy. Previous studies have similarly suggested that, after the onset of senescence, sarcopenia results in a loss in overall muscle mass (Rosenberg, 1997; Cruz-Jentoft et al., 2010) which may decrease force production capacity. The oldest individuals studied by Chazeau and colleagues (2012) were just above the threshold of senescence; as our study incorporates individuals of more advanced ages, we predict that we will be able to more fully demonstrate the effects of senescence on the PCSA of the jaw adductors (which are responsible for the production of bite force) and anticipate that it will decline in animals over the age of 5.5 years old.

H3: Muscle fascicle length increases throughout postnatal development until adult size is reached and remains relatively constant throughout adulthood, then decreases after the onset of senescence.

Muscle fascicles increase in length throughout postnatal development (Goldspink, 1980). This increase in length is the result of an increase in the number of sarcomeres present in each fiber and not due to an increase in the length of the sarcomeres already present (Elliott and Crawford, 1965; Close, 1972; Goldspink, 1980). Based on this expectation, we hypothesize that fascicle length increases with body size from birth until the cessation of growth which occurs around the age of 6 months (Castanet et al., 2004). After this period, we expect the length of the muscle fascicles to remain relatively constant until senescence. A study conducted by Narici and colleagues (2003) evaluated the effects of aging on human gastrocnemius medialis muscle and observed reductions in PCSA, fascicle length, and pennation angles in elderly men (Narici et al., 2003). This suggests that sarcopenia is not only characterized by a loss of muscle mass but also a loss of sarcomeres which results in a decrease in fascicle length (Narici et al., 2003).

MATERIALS AND METHODS

Sample

To test these hypotheses, we dissected thirty-three (23 males and 10 females) *M. murinus* ranging in age from six days to eight years of age (Table S1). The animals were born and raised in captivity in the laboratory breeding colony located in Brunoy, France (license number # F91-

114-1). None of these animals were euthanized for the purpose of this study. The specimens had been previously fixed in ten percent formalin and stored in seventy percent ethanol. This is the largest intraspecific sample of any primate to have been evaluated for ontogenetic muscle fiber architecture changes.

We divided our sample into four age-cohorts, infant, juvenile, adult, and senescent, based on the life history of captive *Microcebus murinus.* The infant cohort consisted of individuals less than two months of age (pre-weaning; Castanet et al., 2004). Individuals between the age of two and nine months old to the approximate age of sexual maturity (Lutermann et al., 2006) were classified as juveniles. Individuals over the age of nine months but younger than 5.5 years were classified as adults and individuals over 5.5 years of age were classified as senescent (Chazeau et al., 2012).

Gross Dissection

Following careful skinning, we removed all three of the mandibular adductors (the masseter, temporalis, and medial pterygoid; Fig. 1). When feasible, each constituent muscle portion (e.g., superficial, deep and zygomatic (i.e., zygomaticomandibularis) portions of masseter, and temporalis) were excised individually; however, in instances in which the muscle bellies had become fused, muscle portions were removed as one. The mass of each muscle portion was recorded immediately following excision.

Chemical Dissection

A protocol modified from Rayne and Crawford (1972) was utilized to chemically dissect the muscles. The excised muscles were placed individually into a 35% aqueous nitric acid solution to dissolve the connective tissue binding their fascicles, until fascicles could be teased apart without damage. This process took 12-24 hours depending on the size and amount of connective tissue in and surrounding the muscle. Once fascicles could be teased apart, muscles were transferred into 50% aqueous glycerol to neutralize the reaction and cease further chemical digestion. The separated muscle fascicles were arranged such they were lying flat and photographed, alongside a scale bar, using a Nikon D3000 camera. Fascicle lengths were subsequently measured using the software package ImageJ (IJ1.46r). When available, we measured a minimum of 40 muscle fibers per muscle in order to calculate a representative fascicle length; though some smaller muscles had fewer measurable fascicles.

Data Analysis

Using the muscle mass and average fascicle length for each muscle, we calculated the physiological cross-sectional area (PCSA)—an estimator of force production using the following formula modified from (Schumacher, 1961):

$$\text{PCSA} = \frac{\text{muscle mass(g)}}{\text{avg. fascicle length (cm)} * \text{specific density of muscle (g/cm}^3\text{)}}$$

The specific density of mammalian skeletal muscle used was a constant of 1.0564 g/cm^3, following Murphy and Beardsley (1974) . To evaluate the total adductors as a single functional unit, we then calculated three aggregate measures: total muscle mass, total PCSA and weighted average fascicle length. Total muscle mass and total PCSA were calculated by summing the individual components. An average weighted fascicle length was calculated by using the following formula adapted from (Hartstone-Rose et al., 2012):

$$FL_X = \frac{(FL_{SM}\, m_{SM}) + (FL_{DM}\, m_{DM}) + (FL_{ZM}\, m_{ZM}) + (FL_{ST}\, m_{ST}) + (FL_{DT}\, m_{DT}) + (FL_{ZT}\, m_{ZT}) + (FL_{MP}\, m_{MP})}{(m_{SM} + m_{DM} + m_{ZM} + m_{ST} + m_{DT} + m_{ZT} + m_{MP})}$$

where FL_X is the weighted fascicle length and FL_{SM}, FL_{DM}, FL_{ZM}, FL_{ST}, FL_{DT}, FL_{ZT}, FL_{MP}, are the average fascicle length and m_{SM}, m_{DM}, m_{ZM}, m_{ST}, m_{DT}, m_{ZT}, m_{MP} are the muscle masses for the superficial masseter, deep masseter, zygomaticomandibularis, superficial temporalis, deep temporalis, zygomatic temporalis, and medial pterygoid respectively.

Dental wear state was determined using lateral photographs collected during dissection for some individuals. We designated maturity and dental wear on a five-point scale: 1 = infant

(prior to M-1 eruption); 2 = juvenile (post M-1 eruption but prior to M-3 eruption); 3 = dentally mature with slight dental wear; 4 = dentally mature with moderate dental wear; 5 – dentally mature with heavy dental wear.

Statistical analyses of all variables were conducted using JMP Pro 13 (SAS). All variables were first linearized to a consistent power (i.e., the cubic- and square-roots of the volumetric variables of mass and square variables of areas were taken respectively) and logged. We then conducted curvilinear regressions (polynomial fit degree = 2) for each architectural variable against both age and body mass. To further clarify the ontogenetic trends observed, we calculated the mean for each architectural variable for each age-cohort and then determined the slopes between each mean point to determine the magnitude of change between infancy and juvenility, juvenility and adulthood and adulthood and senescence. Additionally, we evaluated the relationship between dental wear and PCSA, as well as between dental wear and age.

RESULTS

Physiological Cross-Sectional Area

When the PCSA of each mandibular adductor was regressed against age, quadratic curvilinear relationships yielded significant p-values<0.05 (Fig. 2). Equations for each of the

fitted curves shown in Figures 1-5 are provided in supplementary materials (Table S2). This suggests that the PCSA of the adductors increases and peaks in mid-to-late adulthood (supporting H1) before plateauing during senescence (refuting H2). This trend is further indicated by analyzing the slope of total adductor PCSA between the mean points for each group (Table 1): while the slopes from infancy to juvenility and juvenility to adulthood are both clearly positive (0.272 and 0.169, respectively), the slope from adulthood to senescence is essentially nil (0.035). This trend is consistent within both the temporalis and the masseter; however, a negative senescent slope (-0.233) is observed for the medial pterygoid, suggesting a decline in the force production of this muscle within older individuals. However, the decline observed in this muscle may be exaggerated by a single adult specimen with an exceptionally high medial pterygoid PCSA, which inflates the adult mean (slope with individual excluded= 0.0806).

Muscle Mass

When regressing adductor mass against age, a quadratic curvilinear relationship was observed to be significant in each case with p-values <0.01 (Fig. 3). Muscle mass of the mandibular adductors increases and peaks during early to mid-adulthood (supporting H1) and plateaus into senescence (refuting H2). This trend is also observed when evaluating the slopes between each age cohort within the total adductor and temporalis mass. Masseter displays a similar trend, though with an earlier plateau occurring between juvenility and adulthood (Table

1). However, as for its PCSA, the medial pterygoid exhibits a distinctive trend, with a steep decline (slope= -0.397) in muscle mass from adulthood to senescence (Fig. 3d, Table 1). This decline, again, may have been exaggerated by the inclusion of one adult individual with an exceptionally massive medial pterygoid (slope with individual excluded= -0.224).

Fascicle Length

When the logged weighted average fascicle length and the average fascicle length from each individual adductor are regressed with log age, quadratic curvilinear relationships are significant, with $p < 0.01$ (Fig. 4). For weighted average fascicle lengths, an increase is observed from infants to juveniles (partially supporting H3), but this trend plateaus through all further ages (partially refuting H3; Table 1). The same trend is observed for the temporalis alone. In the case of the masseter and the medial pterygoid, however, average fascicle lengths show a slight increase through to adulthood, before decreasing into senescence (Table 1). This decline is particularly pronounced within the medial pterygoid (slope = -0.168; Table 1).

Body Mass

A significant curvilinear relationship is observed when body mass is regressed against age, with $p < 0.0001$ (Fig. 5). This trend reflects a rapid increase in body mass occurring

throughout infancy and juvenility, which peaks in the early stages of adulthood. Following this, a decline in body mass is associated with the onset of senescence.

DISCUSSION

Masticatory muscle fiber architecture has been a growing focus of anatomical research over the last several decades. Our study is one of the first to comprehensively evaluate the fiber architecture within all of the mandibular adductors in a large intraspecific sample with known ages; it is the largest intraspecific primate sample for which the ontogeny of muscle fiber architecture has been evaluated. This allowed thorough investigation into the ontogenetic changes that occur within the fiber architecture of the mandibular adductors within *M. murinus*.

Based on the need for increased force production capabilities as the feeding mechanism transitions from suckling to chewing, we hypothesized that PCSA would increase throughout early ontogeny in *M. murinus*, driven largely by an increase in muscle mass. Our findings support this hypothesis (H1). Physiological cross-sectional area increased throughout infancy and juvenility then plateaued during adulthood; a trend which closely mirrored the changes in muscle mass. However, we further predicted a decline in PCSA associated with the onset of senescence, following the functional analysis of the ontogeny of bite force in *M. murinus* by

Chazeau and colleagues (2012). The findings of our study did not support this hypothesis (H2): rather, PCSA remains relatively consistent between our adult and senescent groups. When looking at the bivariate plots of the log PCSA for each mandibular adductor against log age, the plateau during adulthood is relatively apparent (Fig. 2); however, the anticipated point of inflection associated with senescence is not. The exception to this trend was the medial pterygoid which displays a notable shift in both mass and PCSA during senescence, with both variables showing a marked decline.

These findings appear curious in light of the findings of Chazeau and colleagues (2012) that bite force was reduced within senescent individuals of *M. murinus*. Despite this functional separation, there is no clear physiological decline in the force production capacity of the adductor muscles between prime-age and senescent individuals. Consequently, other factors may therefore be limiting bite force production within senescent individuals, such as a decline in motor coordination or perhaps even a behaviorally reduced willingness to bite with relative maximal force. The maxillae and mandibles of older individuals do, based on qualitative observation, seem to be more lightly built (e.g., osteoporotic). It is therefore possible that older individuals are less capable of safely transmitting the forces associated with maximal biting through this region of the skull, and thus adjust their behavior to prevent micro- or macro-damage to the facial skeleton. Future work could explore this phenomenon in greater depth through the use of CT scanning to examine bone density and produce finite-element models to

evaluate jaw resistance to deformation at differing bone densities (e.g., Röhrle and Pullan, 2007).

In terms of fascicle lengths, we observed that adult lengths were attained early during development, and remained relatively constant throughout the animal's life span, across the adductor musculature. This trend partially supports our hypothesis in that the fascicle lengths increased until adult size was reached, which occurs around six months of age (H3). However, this observation also refutes our hypothesis (H3) that fascicle lengths would experience a decrease in length at the onset of senescence contradicting a study conducted by Narici and colleagues (2003) which characterized sarcopenia as not just a loss in muscle mass but also a subsequent loss in sarcomeres. If sarcomeres were lost in our sample, it appears that the loss was entirely in parallel fibers (i.e., cross-section/mass) and not in serial (i.e., no shortening of fascicles).

Overall, we anticipated quadratic models to be significant because for each architectural property, we expected a rapid increase through infancy and juvenility, a plateau occurring in adulthood, and a decline with senescence. Although the clear points of inflection we expected to see in late adulthood to early senescence were not obvious in most cases, quadratic curvilinear relationships were observed to be significant when each architectural variable was regressed with age.

From these results, representing the most comprehensive ontogenetic and intraspecific samples of primate masticatory muscle architecture, we have characterized myological changes across the lifespan of *M. murinus*. Our findings suggest that the changes in PCSA are driven mostly by changes in muscle mass including growth through early adulthood, and a plateau into senescence, whereas masticatory fascicle lengths remain surprisingly constant throughout life. Future studies are needed to determine whether or not these trends are consistent throughout other muscular regions and if these findings are species specific.

ACKNOWLEDGEMENTS

We would like to express our sincere gratitude to the staff at the colony of Brunoy at the Muséum National d'Histoire Naturelle for allowing us access to such a rare and outstanding sample of these amazing primates. Specifically, we would like to thank Martine Perret and all the animal care technicians. We would also like to thank Isabelle Hardy for maintaining the colony data base and for providing us with ages of the specimens. Additionally, we would like to thank both of our anonymous reviewers and editor, Timothy Smith, for their feedback. This project was supported by the National Science Foundation (IOS-15-57125 and BCS-14-40599).

LITERATURE CITED

Anapol F, Barry K. 1996. Fiber architecture of the extensors of the hindlimb in semiterrestrial and arboreal guenons. Am J Phys Anthropol 99:429-447.

Anapol F, Shahnoor N, Ross CF. 2008. Scaling of reduced physiologic cross-sectional area in primate muscles of mastication. In: Primate craniofacial function and biology: Springer. p 201-216.

Antón SC. 1999. Macaque masseter muscle: internal architecture, fiber length and cross-sectional area. Int J Primatol 20:441-462.

Antón SC. 2000. Macaque pterygoid muscles: internal architecture, fiber length, and cross-sectional area. International Journal of Primatology 21:131-156.

Bons N, Rieger F, Prudhomme D, Fisher A, Krause KH. 2006. *Microcebus murinus*: a useful primate model for human cerebral aging and Alzheimer's disease? Genes Brain Behav 5:120-130.

Cachel S. 1984. Growth and allometry in primate masticatory muscles. Arch Oral Biol 29:287-293.

Carlson DS. 1983. Growth of the masseter muscle in rhesus monkeys (*Macaca mulatta*). Am J Phys Anthropol 60:401-410.

Castanet J, Croci S, Aujard F, Perret M, Cubo J, De Margerie E. 2004. Lines of arrested growth in bone and age estimation in a small primate: *Microcebus murinus*. J Zool 263:31-39.

Chazeau C, Marchal J, Hackert R, Perret M, Herrel A. 2012. Proximate determinants of bite force capacity in the mouse lemur. J Zool 290:42-48.

Close R. 1972. Dynamic properties of mammalian skeletal muscles. Physiol Rev 52:129-197.

Cruz-Jentoft AJ, Baeyens JP, Bauer JM, Boirie Y, Cederholm T, Landi F, Martin FC, Michel J-P, Rolland Y, Schneider SM, Topinková E, Vandewoude M, Zamboni M. 2010. Sarcopenia: European consensus on definition and diagnosis. Age Ageing 39:412-423.

Curtis AA, Santana SE. 2018. Jaw-dropping: functional variation in the digastric muscle in bats. Anat Rec 301:279-290.

Dammhahn M, Kappeler PM. 2008. Comparative feeding ecology of sympatric *Microcebus berthae* and *M. murinus*. Int J Primatol 29:1567.

Dickinson E, Fitton LC, Kupczik K. 2018. Ontogenetic changes to muscle architectural properties within the jaw-adductor musculature of *Macaca fascicularis*. Am J Phys Anthropol 167:291-310.

Dumont ER, Herrel A, Medellin RA, Vargas-Contreras JA, Santana SE. 2009. Built to bite: cranial design and function in the wrinkle-faced bat. J Zool 279:329-337.

Elliott D, Crawford G. 1965. The thickness and collagen content of tendon relative to the cross-sectional area of muscle during growth. Proc R Soc Lond B 162:198-202.

Eng CM, Ward SR, Vinyard CJ, Taylor AB. 2009. The morphology of the masticatory apparatus facilitates muscle force production at wide jaw gapes in tree-gouging common marmosets (*Callithrix jacchus*). J Exp Biol 212:4040.

Ezran C, Karanewsky CJ, Pendleton JL, Sholtz A, Krasnow MR, Willick J, Razafindrakoto A, Zohdy S, Albertelli MA, Krasnow MA. 2017. The mouse lemur, a genetic model organism for primate biology, behavior, and health. Genetics 206:651.

Fabre PH, Herrel A, Fitriana Y, Meslin L, Hautier L. 2017. Masticatory muscle architecture in a water-rat from Australasia (Murinae, *Hydromys*) and its implication for the evolution of carnivory in rodents. J Anat 231:380-397.

Gans C. 1982. Fiber architecture and muscle function. Exerc Sport Sci Rev 10:160-207.

Gans C, Bock WJ. 1965. The functional significance of muscle architecture--a theoretical analysis. Ergeb Anat Entwicklungsgesch 38:115-142.

Gans C, Gaunt AS. 1991. Muscle architecture in relation to function. J Biomech 24:53-65.

Goldspink G. 1980. Growth of muscle. Development and specialization of skeletal muscle:19-35.

Hartstone-Rose A, Perry JMG, Morrow CJ. 2012. Bite force estimation and the fiber architecture of felid masticatory muscles. Anat Rec 295:1336-1351.

Hartstone-Rose A, Deutsch AR, Leischner CL, Pastor F. 2018. Dietary correlates of primate masticatory muscle fiber architecture. Anat Rec 301:311-324.

Herrel A, De Smet A, Aguirre LF, Aerts P. 2008. Morphological and mechanical determinants of bite force in bats: do muscles matter? J Exp Biol 211:86-91.

Huhov J, Henry-Ward W, Phillips L, German R. 1988. Growth allometry of craniomandibular muscles, tendons, and bones in the laboratory rat (*Rattus norvegicus*): Relationships to oromotor maturation and biomechanics of feeding. Am J Anat 182:381-394.

Knuttgen HG. 1976. Development of muscular strength and endurance. In: Neuromuscular mechanisms for therapeutic and conditioning exercise. p 97-118.

Langenbach GEJ, Weijs WA. 1990. Growth patterns of the rabbit masticatory muscles. J Dent Res 69:20-25.

Leischner CL, Crouch M, Allen KL, Marchi D, Pastor F, Hartstone-Rose A. 2018. Scaling of primate forearm muscle architecture as it relates to locomotion and posture. Anat Rec 301:484-495.

Lieber RL, Friden J. 2000. Functional and clinical significance of skeletal muscle architecture. Muscle Nerve 23:1647-1666.

Lutermann H, Schmelting B, Radespiel U, Ehresmann P, Zimmermann E. 2006. The role of survival for the evolution of female philopatry in a solitary forager, the grey mouse lemur (*Microcebus murinus*). Proc R Soc B 273:2527-2533.

Martin R. 1971. A laboratory breeding colony of the lesser mouse lemur. In: Breeding primates: Karger Publishers. p 161-171.

Maughan RJ, Watson JS, Weir J. 1983. Strength and cross-sectional area of human skeletal muscle. J Physiol 338:37-49.

Mittermeier RA, Louis EE, Richardson M, Schwitzer C, Langrand O, Rylands AB, Hawkins F, Rajaobelina S, Rasimbazafy J, Rasoloarison RM, Roos C, Kappeler PM, Mackinnon J. 2010. Lemurs of Madagascar, Third ed. Arlington, Virginia: Conservation International.

Murphy RA, Beardsley AC. 1974. Mechanical properties of the cat soleus muscle in situ. The Am J Physiol 227:1008-1013.
Narici MV, Maganaris CN, Reeves ND, Capodaglio P. 2003. Effect of aging on human muscle architecture. J Appl Physiol 95:2229-2234.
Otten E. 1988. Concepts and models of functional architecture in skeletal muscle. Exerc Sport Sci Rev 16:89-138.
Perret M. 1997. Change in photoperiodic cycle affects life span in a prosimian primate (*Microcebus murinu*s). J Biol Rhythms 12:136-145.
Perry JMG, Hartstone-Rose A. 2010. Maximum ingested food size in captive strepsirrhine primates: Scaling and the effects of diet. Am J Phys Anthropol 142:625-635.
Perry JMG, Hartstone-Rose A, Wall CE. 2011. The jaw adductors of strepsirrhines in relation to body size, diet, and ingested food size. Anat Rec 294:712-728.
Perry JMG, Macneill KE, Heckler AL, Rakotoarisoa G, Hartstone-Rose A. 2014. Anatomy and adaptations of the chewing muscles in *Daubentonia* (Lemuriformes). Anat Rec 297:308-316.
Perry JMG, Wall CE. 2008. Scaling of the chewing muscles in prosimians. In: Primate craniofacial function and biology: Springer. p 217-240.
Pfaller JB, Gignac PM, Erickson GM. 2011. Ontogenetic changes in jaw-muscle architecture facilitate durophagy in the turtle *Sternotherus minor*. J Exp Biol 214:1655-1667.
Pfaller JB, Herrera ND, Gignac PM, Erickson GM. 2009. Ontogenetic scaling of cranial morphology and bite-force generation in the loggerhead musk turtle. J Zool 280:280-289.
Prufrock KA, Perry JMG. 2018. Strepsirrhine diets and the pattern of masticatory muscle development. FASEB J 32:780-785.
Rassoul RA, Alves S, Pantesco V, De Vos J, Michel B, Perret M, Mestre-Frances N, Verdier J-M, Devau G. 2010. Distinct transcriptome expression of the temporal cortex of the primate *Microcebus murinus* during brain aging versus Alzheimer's disease-like pathology. PLoS One 5:e12770.
Rayne J, Crawford GNC. 1972. The relationship between fibre length, muscle excursion and jaw movements in the rat. Arch Oral Biol 17:859-IN811.
Röhrle O, Pullan AJ. 2007. Three-dimensional finite element modelling of muscle forces during mastication. J Biomech 40:3363-3372.
Rosenberg IH. 1997. Sarcopenia: origins and clinical relevance. J Nutr 127:990S-991S.
Santana SE. 2018. Comparative anatomy of bat jaw musculature via diffusible iodine-based contrast-enhanced computed tomography. Anat Rec 301:267-278.
Santana SE, Cheung E. 2016. Go big or go fish: morphological specializations in carnivorous bats. Proc R Soc B 283:20160615.
Schumacher G-H. 1961. Funktionelle morphologie der kaumuskulatur: G. Fischer.
Taylor AB, Jones KE, Kunwar R, Ravosa MJ. 2006. Dietary consistency and plasticity of masseter fiber architecture in postweaning rabbits. Anat Rec 288:1105-1111.

Taylor AB, Vinyard CJ. 2009. Jaw-muscle fiber architecture in tufted capuchins favors generating relatively large muscle forces without compromising jaw gape. J Hum Evol 57:710-720.

FIGURE LEGEND

Figure 1. Muscles of mastication of Microcebus murinus shown in situ. Legend: ST= superficial temporalis, ZT= zygomatic temporalis, DT= deep temporalis, SM= superficial masseter, ZM= zygomaticomandibularis, DM= deep masseter, LP= lateral pterygoid, MP= medial pterygoid.

Figure 2. Bivariate plots of the log PCSA (cm^2)^(1/2) of total sum and each separate mandibular adductor regressed against log age. Legend: open circles = infants, open triangles = juveniles, open squares = adults, x = senescents, closed shapes = mean for their respective age cohorts (closed diamonds = mean for senescent individuals). The vertical lines indicate the boundaries between the following life history stages: infant-juvenile, juvenile-adult, and adult-senescent.

Figure 3. Bivariate plots of the log MM (g)^(1/3) of total sum and each separate mandibular adductor regressed against log age. Legend: same as Figure 2.

Figure 4. Bivariate plots of the log FL (cm) weighted average of combined adductors and of each mandibular adductor regressed against log age. Legend same as in Fig. 2.

Figure 5. Bivariate plot of log BM (g)^(1/3) regressed against log age. Legend same as in Fig. 2.

Table 1. Slopes calculated between the mean of each age cohort infancy to juvenility, juvenility to adult and adult to senescence for each architectural variable of each mandibular adductor.

Muscle(s)	Age Cohort Range	PCSA Slope	MM Slope	FL Slope
Total Adductors	Infant − Juvenile	0.272	0.202	0.172
	Juvenile − Adult	0.169	0.116	0.012
	Adult − Senescent	0.035	0.031	-0.002
Total Masseter	Infant − Juvenile	0.275	0.364	0.031
	Juvenile − Adult	0.174	0.004	0.087
	Adult − Senescent	0.079	0.042	-0.028
Temporalis	Infant − Juvenile	0.276	0.217	0.184
	Juvenile − Adult	0.151	0.101	0.007
	Adult − Senescent	0.091	0.059	-0.019
Medial Pterygoid	Infant − Juvenile	0.257	0.185	0.105
	Juvenile − Adult	0.202	0.155	0.097
	Adult − Senescent	-0.233	-0.397	-0.168

Supplemental Materials

Table S1. Ontogenetic sample obtained from the Muséum National d'Histoire Naturelle in Paris, France by age.

	Specimen ID	Sex	Age (years)	Body Mass (g)
Infant	Infant from	F	0.014	6

(N=4; F=1; M=3)	119EB			
	Infant from 162H	M	0.03	10
	Infant from 172IB	M	0.11	36
	Infant from 276B	M	0.16	41
Juvenile (N=4; F=3; M=1)	Infant from 943GF	F	0.22	38
	102CA	F	0.36	50
	147EE	M	0.37	98
	276AC	F	0.5	52
Adult (N=13; F=5; M=8)	139BB	M	0.97	87
	278ACC	F	2	78
	911FBJ	F	2.22	128
	219E	M	2.38	102
	241AA	M	2.79	62
	189GAA	M	3.33	81
	119CBB	M	3.66	91
	893AAJ	M	3.66	116
	153F	F	3.92	86
	206DBA	M	3.93	80
	921BAC	F	4.42	136

	989EB	F	4.7	118
	225A	M	5.42	86
Senescent (N=9; F=1; M=8)	143CAD	M	5.88	74
	143CAC	M	5.92	73
	163DE	M	5.95	90
	100DBA	M	6	70
	223A	M	6.2	66
	113B	M	6.28	53
	245BB	F	7	56
	143CAA	M	7.01	96
	883DEM	M	8	98
Unknown (N=3; F=0; M=3)	No number 1	M	unknown	78
	No number 2	M	unknown	82
	Z93265	M	unknown	68

Table S2. Equations for each of the fitted curves from each of the bivariate plots.

Regression	Equation for Fitted Curve
Log Adductor PCSA vs Log Age	Log Adductor PCSA (cm^2)^(1/2) = -0.027397 + 0.1318052*Log Age (years) - 0.1051152*(Log Age(years)-0.15951)^2
Log Total Masseter PCSA vs Log Age	Log Total Masseter PCSA (cm^2)^(1/2) = -0.22908 + 0.1416485*Log Age (years) - 0.0949447*(Log Age (years)-0.15951)^2
Log Temp. PCSA vs Log Age	Log Temp. PCSA (cm^2)^(1/2) = -0.21628 +0.1432414*Log Age (years) - 0.1060308*(Log Age (years)-0.15951)^2
Log MP PCSA vs Log Age	Log MP PCSA (cm^2)^(1/2) = -0.449909 +0.1112891*Log Age (years) - 0.1375233*(Log Age (years)-0.15951)^2
Log Adductor MM vs Log Age	Log Adductor Mass (g)^(1/3) = -0.124065 + 0.0738649*Log Age (years) - 0.0956959*(Log Age (years)-0.24489)^2
Log Total Masseter MM vs Log Age	Log Total Masseter Mass (g)^(1/3) = -0.248976 + 0.0593702*Log Age (years) - 0.0941387*(Log Age (years)-0.24489)^2
Log Temp. MM vs Log Age	Log Temp. Mass (g)^(1/3) = -0.221721 + 0.0763819*Log Age (years) - 0.1002467*(Log Age (years)-0.24489)^2
Log MP MM vs Log Age	Log MP Mass (g)^(1/3) = -0.466223 - 0.0245*Log Age (years) - 0.1658636*(Log Age (years)-0.24489)^2
Log Adductor FL vs Log Age	Log Adductor FL (cm) = -0.328099 - 0.0089892*Log Age (years) - 0.0720451*(Log Age (years)-0.24489)^2
Log Total Masseter FL vs Log Age	Log Total Masseter FL (cm) = -0.38599 + 0.0174315*Log Age (years) - 0.0416161*(Log Age (years)-0.24489)^2
Log Temp. FL vs Log Age	Log Temp. FL (cm) = -0.263754 - 0.0211211*Log Age (years) - 0.0886747*(Log Age (years)-0.24489)^2
Log MP FL vs Log Age	Log MP FL (cm) = -0.542119 - 0.0563075*Log Age (years) - 0.1244758*(Log Age (years)-0.24489)^2
Log BM vs Log Age	Log BM (g)^(1/3) = 0.6474901 + 0.0173246*Log Age (years) - 0.0850562*(Log Age (years)-0.24489)^2

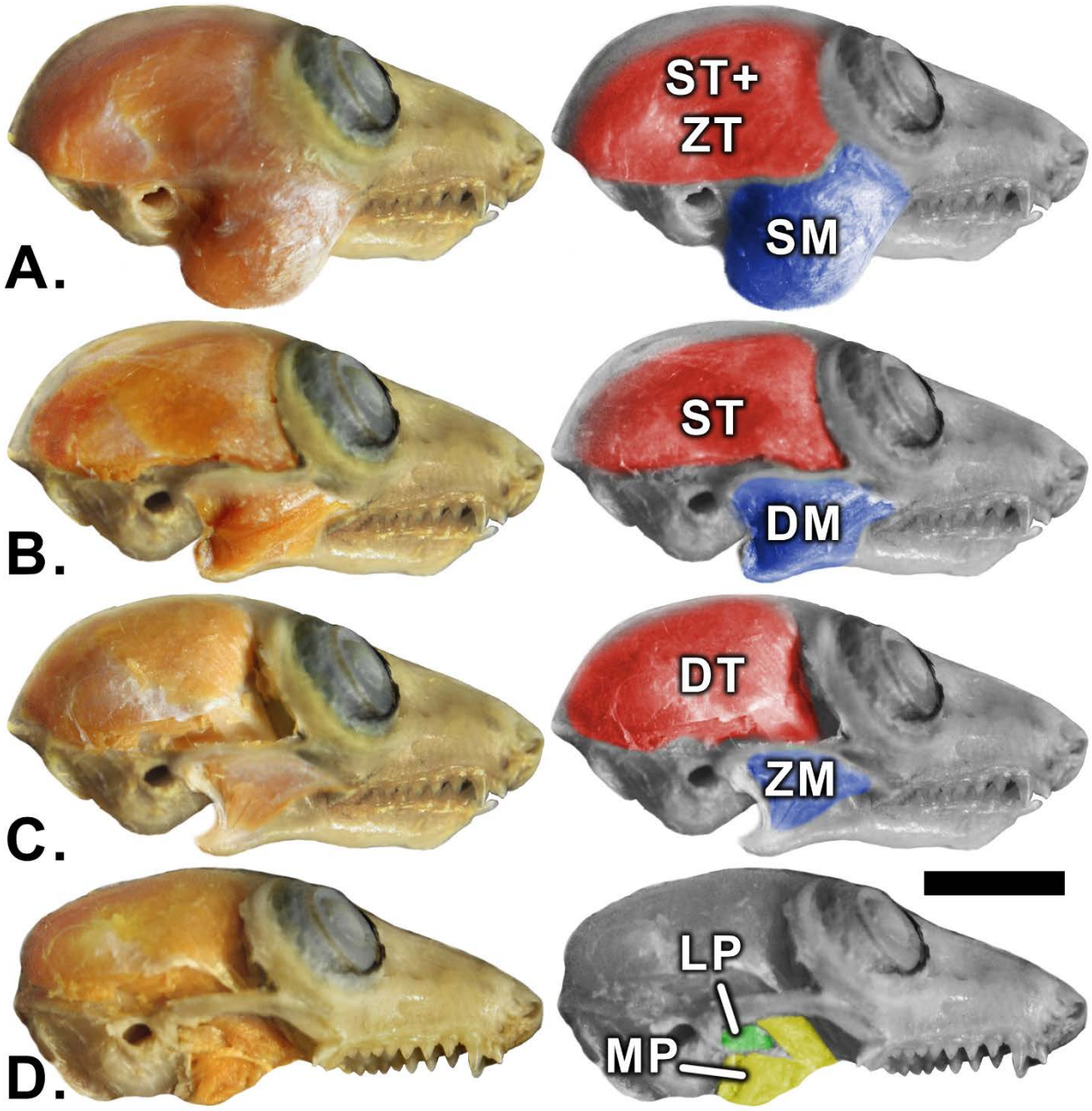

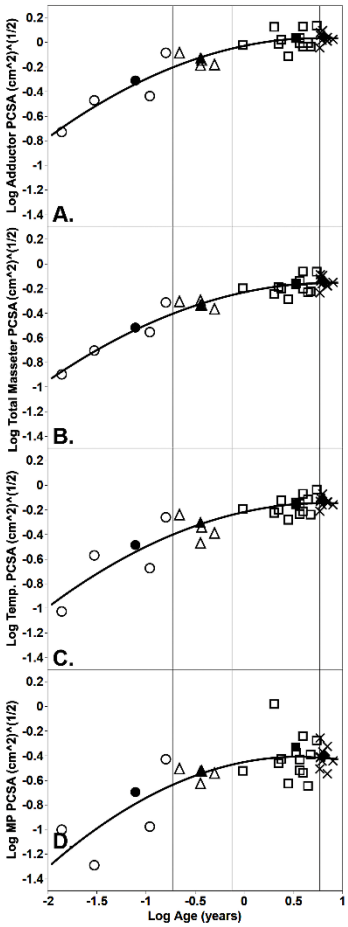

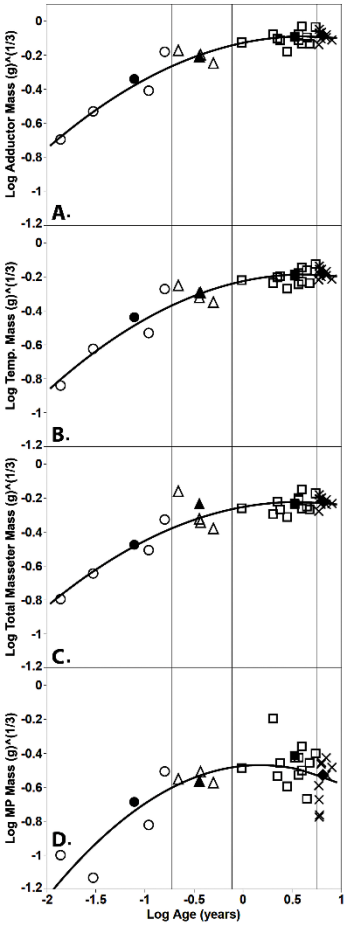

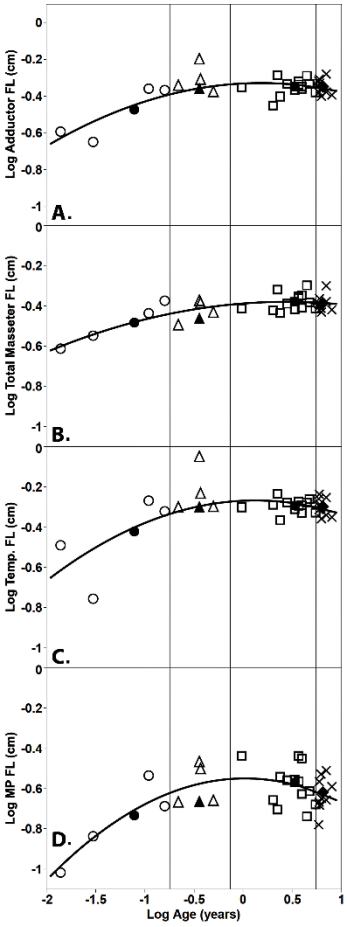

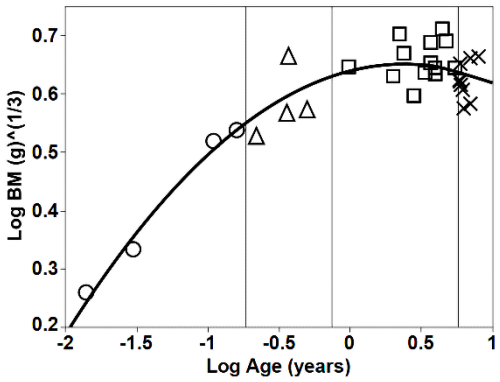

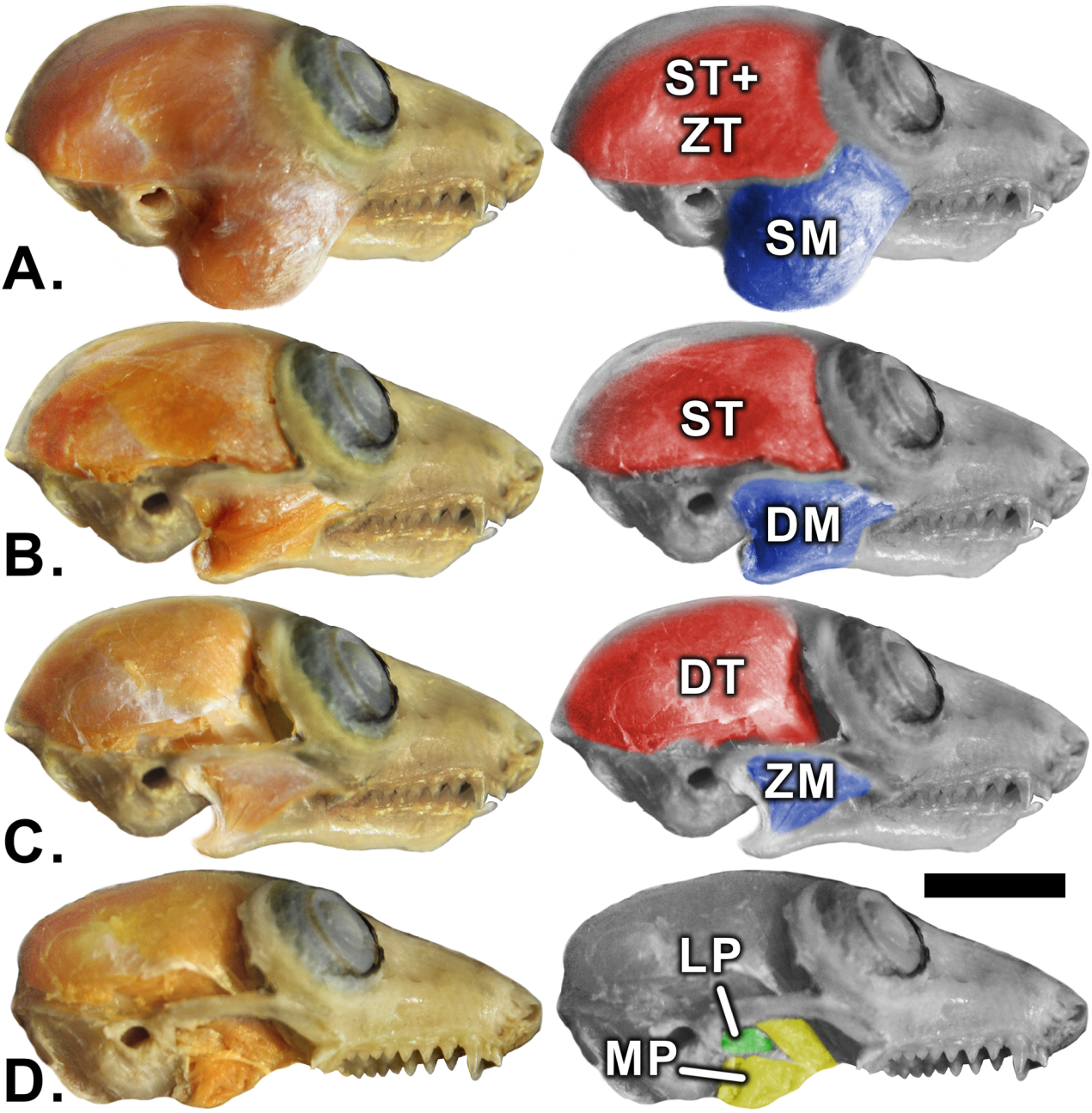

AR_24259_Figure 1.tif

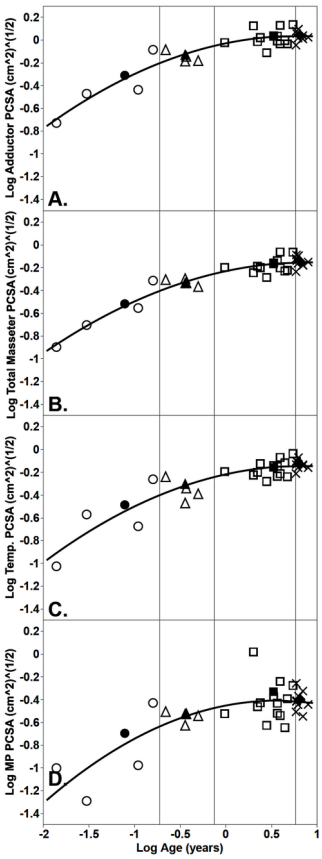

AR_24259_Figure_2.tif

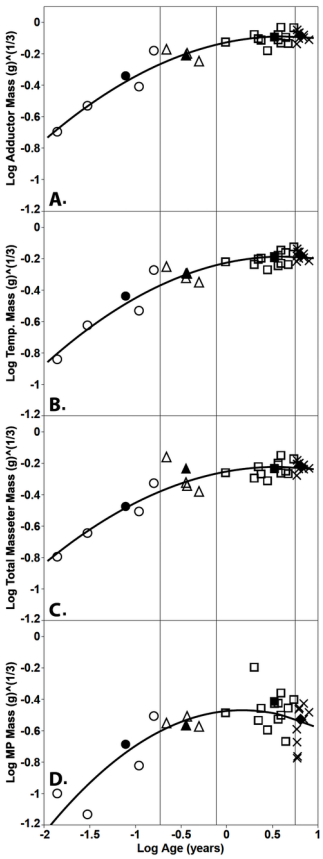

AR_24259_Figure_3.tif

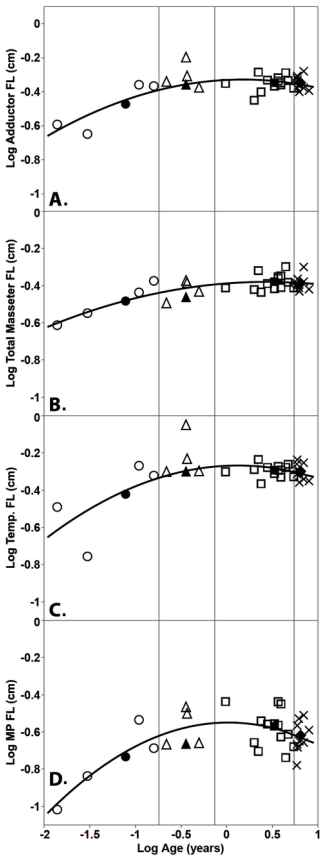

AR_24259_Figure_4.tif

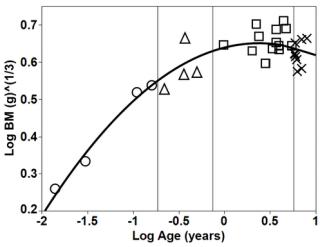

AR_24259_Figure_5.tif

Table 1. Slopes calculated between the mean of each age cohort infancy to juvenility, juvenility to adult and adult to senescence for each architectural variable of each mandibular adductor.

Muscle(s)	Age Cohort Range	PCSA Slope	MM Slope	FL Slope
Total Adductors	Infant − Juvenile	0.272	0.202	0.172
	Juvenile − Adult	0.169	0.116	0.012
	Adult − Senescent	0.035	0.031	-0.002
Total Masseter	Infant − Juvenile	0.275	0.364	0.031
	Juvenile − Adult	0.174	0.004	0.087
	Adult − Senescent	0.079	0.042	-0.028
Temporalis	Infant − Juvenile	0.276	0.217	0.184
	Juvenile − Adult	0.151	0.101	0.007
	Adult − Senescent	0.091	0.059	-0.019
Medial Pterygoid	Infant − Juvenile	0.257	0.185	0.105
	Juvenile − Adult	0.202	0.155	0.097
	Adult − Senescent	-0.233	-0.397	-0.168

Supplemental Materials

Table S1. Ontogenetic sample obtained from the Muséum National d'Histoire Naturelle in Paris, France by age.

	Specimen ID	Sex	Age (years)	Body Mass (g)
Infant (N=4; F=1; M=3)	Infant from 119EB	F	0.014	6
	Infant from 162H	M	0.03	10

	Infant from 172IB	M	0.11	36
	Infant from 276B	M	0.16	41
Juvenile (N=4; F=3; M=1)	Infant from 943GF	F	0.22	38
	102CA	F	0.36	50
	147EE	M	0.37	98
	276AC	F	0.5	52
Adult (N=13; F=5; M=8)	139BB	M	0.97	87
	278ACC	F	2	78
	911FBJ	F	2.22	128
	219E	M	2.38	102
	241AA	M	2.79	62
	189GAA	M	3.33	81
	119CBB	M	3.66	91
	893AAJ	M	3.66	116
	153F	F	3.92	86
	206DBA	M	3.93	80
	921BAC	F	4.42	136
	989EB	F	4.7	118
	225A	M	5.42	86
Senescent (N=9; F=1; M=8)	143CAD	M	5.88	74
	143CAC	M	5.92	73
	163DE	M	5.95	90

	100DBA	M	6	70
	223A	M	6.2	66
	113B	M	6.28	53
	245BB	F	7	56
	143CAA	M	7.01	96
	883DEM	M	8	98
Unknown (N=3; F=0; M=3)	No number 1	M	unknown	78
	No number 2	M	unknown	82
	Z93265	M	unknown	68

Table S2. Equations for each of the fitted curves from each of the bivariate plots.

Regression	Equation for Fitted Curve
Log Adductor PCSA vs Log Age	Log Adductor PCSA (cm^2)^(1/2) = -0.027397 + 0.1318052*Log Age (years) - 0.1051152*(Log Age(years)-0.15951)^2
Log Total Masseter PCSA vs Log Age	Log Total Masseter PCSA (cm^2)^(1/2) = -0.22908 + 0.1416485*Log Age (years) - 0.0949447*(Log Age (years)-0.15951)^2
Log Temp. PCSA vs Log Age	Log Temp. PCSA (cm^2)^(1/2) = -0.21628 +0.1432414*Log Age (years) - 0.1060308*(Log Age (years)-0.15951)^2
Log MP PCSA vs Log Age	Log MP PCSA (cm^2)^(1/2) = -0.449909 +0.1112891*Log Age (years) - 0.1375233*(Log Age (years)-0.15951)^2
Log Adductor MM vs Log Age	Log Adductor Mass (g)^(1/3) = -0.124065 + 0.0738649*Log Age (years) - 0.0956959*(Log Age (years)-0.24489)^2
Log Total Masseter MM vs Log Age	Log Total Masseter Mass (g)^(1/3) = -0.248976 + 0.0593702*Log Age (years) - 0.0941387*(Log Age (years)-0.24489)^2
Log Temp. MM vs Log Age	Log Temp. Mass (g)^(1/3) = -0.221721 + 0.0763819*Log Age (years) - 0.1002467*(Log Age (years)-0.24489)^2
Log MP MM vs Log Age	Log MP Mass (g)^(1/3) = -0.466223 - 0.0245*Log Age (years) - 0.1658636*(Log Age (years)-0.24489)^2
Log Adductor FL vs Log Age	Log Adductor FL (cm) = -0.328099 - 0.0089892*Log Age (years) - 0.0720451*(Log Age (years)-0.24489)^2
Log Total Masseter FL vs Log Age	Log Total Masseter FL (cm) = -0.38599 + 0.0174315*Log Age (years) - 0.0416161*(Log Age (years)-0.24489)^2
Log Temp. FL vs Log Age	Log Temp. FL (cm) = -0.263754 - 0.0211211*Log Age (years) - 0.0886747*(Log Age (years)-0.24489)^2
Log MP FL vs Log Age	Log MP FL (cm) = -0.542119 - 0.0563075*Log Age (years) - 0.1244758*(Log Age (years)-0.24489)^2
Log BM vs Log Age	Log BM (g)^(1/3) = 0.6474901 + 0.0173246*Log Age (years) - 0.0850562*(Log Age (years)-0.24489)^2